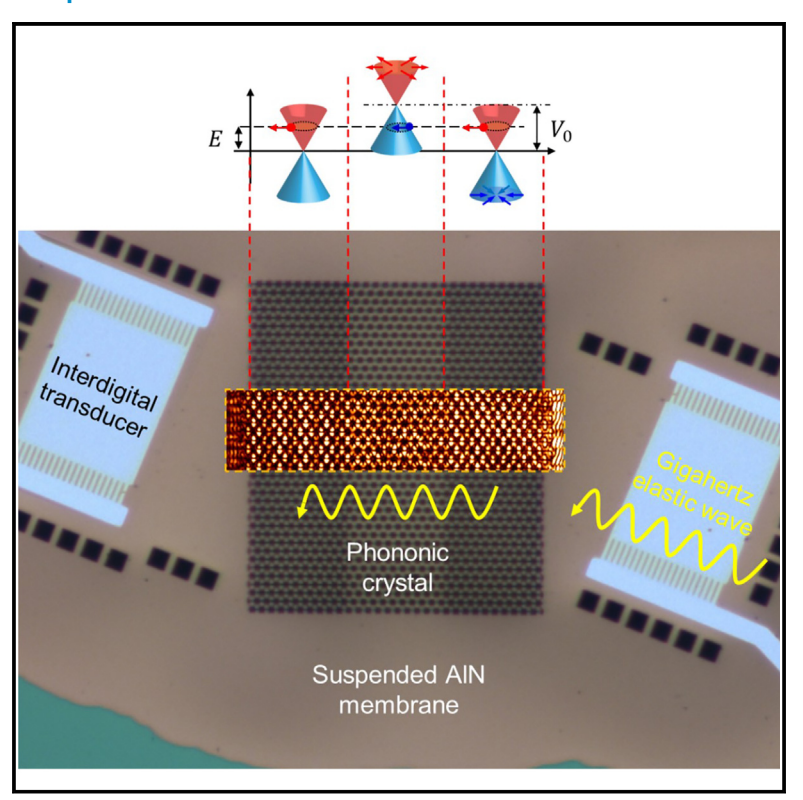
Device

Klein tunneling of gigahertz elastic waves in nanoelectromechanical metamaterials

Graphical abstract



Authors

Daehun Lee, Yue Jiang, Xiaoru Zhang, ..., Qicheng Zhang, A.T. Charlie Johnson, Keji Lai

Correspondence

zhangqicheng@westlake.edu.cn (Q.Z.), cjohnson@physics.upenn.edu (A.T.C.J.), kejilai@physics.utexas.edu (K.L.)

In brief

Klein tunneling of gigahertz elastic waves is realized and observed in a suspended microelectromechanical device. The near-unity transmission and angular dependence of Klein tunneling imaged by transmission-mode microwave impedance microscopy may have applications in classical and quantum information systems.

Highlights

- Nanoscale imaging by transmission-mode microwave impedance microscopy
- Observation of Klein tunneling of gigahertz elastic waves in suspended membranes
- Visualization of angular dependent transmission with group velocity control
- Design of acoustic wave filters with Klein tunneling



Lee et al., 2024, Device 2, 100474 October 18, 2024 © 2024 The Authors. Published by Elsevier Inc. https://doi.org/10.1016/j.device.2024.100474



Please cite this article in press as: Lee et al., Klein tunneling of gigahertz elastic waves in nanoelectromechanical metamaterials, Device (2024), https://doi.org/10.1016/j.device.2024.100474

Device



Article

Klein tunneling of gigahertz elastic waves in nanoelectromechanical metamaterials

Daehun Lee,^{1,8} Yue Jiang,^{2,8} Xiaoru Zhang,¹ Shahin Jahanbani,^{1,7} Chengyu Wen,³ Qicheng Zhang,^{4,5,*} A.T. Charlie Johnson,^{2,6,*} and Keji Lai^{1,9,*}

- ¹Department of Physics, University of Texas at Austin, Austin, TX, USA
- ²Department of Physics and Astronomy, University of Pennsylvania, Philadelphia, PA, USA
- ³Department of Electrical and Systems Engineering, University of Pennsylvania, Philadelphia, PA, USA
- ⁴Research Center for Industries of the Future, Westlake University, Hangzhou, Zhejiang 310030, China
- ⁵Key Laboratory of 3D Micro/Nano Fabrication and Characterization of Zhejiang Province, School of Engineering, Westlake University, Hangzhou, Zhejiang 310030, China
- ⁶Department of Materials Science and Engineering, University of Pennsylvania, Philadelphia, PA, USA
- ⁷Present address: Department of Physics, University of California, Berkeley, Berkeley, CA, USA
- ⁸These authors contributed equally
- ⁹Lead contact
- *Correspondence: zhangqicheng@westlake.edu.cn (Q.Z.), cjohnson@physics.upenn.edu (A.T.C.J.), kejilai@physics.utexas.edu (K.L.) https://doi.org/10.1016/j.device.2024.100474

THE BIGGER PICTURE Gigahertz phonons are emerging as attractive information carriers in signal processing and quantum information applications, with a growing demand to construct long-lived quantum memories. The ever-expanding applications call for precise control of elastic waves in the ultrahigh frequency regime. By applying a concept from high-energy physics known as Klein tunneling, which describes the perfect transmission of a relativistic particle through an energy barrier, we designed a nanoscale on-chip phononic circuit for wave filtering with applications in nanoelectromechanical devices. Furthermore, we realized angle-dependent phonon filtering by engineering group velocity in the reciprocal space. The ability to guide and filter gigahertz phonons is beneficial for enhanced device performance in integrated circuit technology and future quantum information devices.

SUMMARY

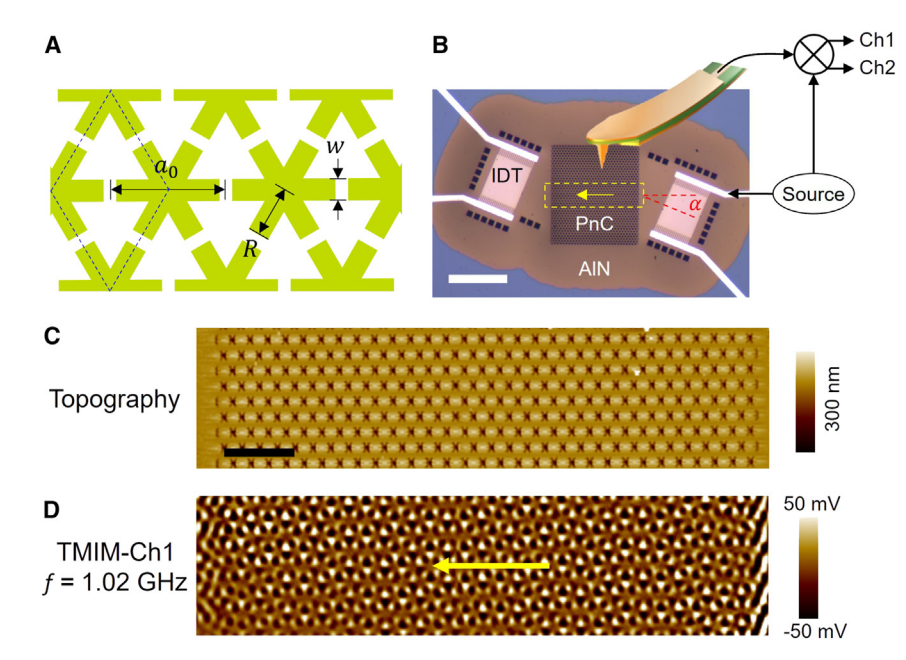
The Klein tunneling effect describes the transmission of a relativistic particle with normal incidence through an energy barrier. It has been observed and tested in various electronic, photonic, and phononic systems, but its potential in guiding and filtering classical waves in the ultrahigh frequency regime has not been explored. Here, we report the realization of acoustic Klein tunneling in a nanoelectromechanical metamaterial system operating at gigahertz frequencies. The piezoelectric potential profiles are obtained by transmission-mode microwave impedance microscopy, from which reciprocal-space maps are extracted. The transmission rate of normally incident elastic waves is near unity in the Klein tunneling regime and drops significantly outside this frequency range, consistent with microwave network analysis. Strong angular dependent transmission is possible by controlling the launching angle of the emitter interdigital transducer. This work broadens the horizon for exploiting high-energy-physics phenomena for practical circuit applications in both classical and quantum regimes.

INTRODUCTION

Electromagnetic waves in photonic systems and acoustic/ elastic waves in phononic systems share many features with electronic waves in condensed matter systems. For instance, the frequency dispersion of engineered metamaterials closely resembles the band structure of solid-state materials.^{1,2} Macroscopic periodic structures can be constructed to test exotic phenomena such as Majorana zero modes^{3,4} and non-Hermitian bands,^{5,6} which are difficult to achieve in real materials. Conversely, quantum physics in condensed matter systems can provide insight on the realization of unusual functionalities in various metamaterials, such as topologically protected transport against structural defects or sharp bends.^{7–10} In this context, the classical analog to the Klein tunneling effect,^{11–13} which describes the unity transmission of a relativistic particle







passing through a potential barrier upon normal incidence, holds promise for waveguiding and filtering applications in photonic and phononic systems.

In elementary quantum mechanics, the transmission probability of a nonrelativistic particle decays exponentially when passing through a classically forbidden region.¹⁴ For relativistic Dirac particles, however, normal transmission is unimpeded regardless of the height and width of the energy barrier because of the effect known as Klein tunneling. 11-13 This process relies on two conditions: (1) the presence of a continuum of negative-kinetic-energy states inside the barrier that matches energy of the incoming states and (2) the conservation of chiral pseudospin (a degree of freedom analogous to electron spin) in a bi-spinor wavefunction, which prohibits backscattering under normal incidence. In the originally proposed particle-physics setting, 11-13 however, the realization of Klein tunneling requires the acceleration of a particle to the relativistic regime and the construction of a parallel barrier, which are experimentally very difficult. As a result, experimental investigations of Klein tunneling have been mostly carried out in graphene, 15,16 where quasiparticles near the chargeneutrality point behave as two-dimensional massless Dirac fermions. 17,18 Signatures of Klein tunneling in this condensed matter platform include the excess resistance across a ballistic P-N junction due to the collimation effect 19-21 and the half-period shift in magneto-conductance oscillations induced by quantum interference between two parallel interfaces.²² Similar theoretical and experimental works have also been performed in photonic systems at optical frequencies^{23,24} and phononic systems at the kilohertz (kHz) range.²⁵⁻²⁸ It is widely accepted that analogs of the Klein tunneling effect, originally proposed as a high-energy physics paradox, can be utilized for enhancing quantum transport 19-22 and manipulating light and sound waves.^{23–28}

In this work, we extend the investigation of phononic Klein tunneling to the gigahertz (GHz) regime, which has potential applications in wireless communication and integrated circuit. The

Figure 1. Phononic crystal design and TMIM experiment

(A) Schematic of the phononic crystal design, where the green snowflake regions are etched away. The dashed rhombus depicts the unit cell. (B) Optical image of the freestanding AIN device overlaid with the TMIM setup. The normal of IDT is tilted from the normal of PnC by an angle α . The scale bar represents 100 μ m.

(C and D) Topographic (C) and TMIM-Ch1 (D) images inside the yellow dashed box in (B). Data are taken on the sample with $R=1.90~\mu m$ at f=1.02~GHz. The scale bar represents 20 μm .

nanoelectromechanical phononic metamaterials are fabricated on freestanding aluminum nitride (AIN) membranes, where graphene-like structures are patterned. Using transmission-mode microwave impedance microscopy (TMIM), ^{29,30} we visualized the real-space profile of the elastic waves, from which phononic band structures in the reciprocal space are obtained

using Fourier transform. Upon normal incidence, near-unity transmission is observed at the center of the Klein tunneling regime, while wave propagation outside this frequency range is strongly attenuated. By controlling the launching angle from interdigital transducers (IDTs), we observe strong angular dependent transmission through the heterostructure, in agreement with theoretical predictions. ^{16,18} Our work represents the first demonstration of Klein tunneling in integrated phononic circuits in the ultrahigh frequency (UHF, 300 MHz–3 GHz) regime, which is desirable for classical signal processing and quantum information systems.

RESULTS AND DISCUSSION

Metamaterial design and device fabrication

The phononic crystal (PnC) structure is based on an acoustic analog of graphene. As illustrated in Figure 1A, the metamaterial is formed by etching away snowflake-like patterns 31 from suspended polycrystalline AlN films whose normal direction is along the c axis defined in conventional crystallography. The choice of polycrystalline AlN is mainly due to its in-plane isotropic properties for implementing acoustic graphene. The freestanding film can minimize acoustic leakage to the substrates. Details of the sample quality and the effect of imperfections on the PnC band structure are included in Note S1. The structure has the $C_{6\nu}$ symmetry (i.e., 6-fold rotations about the center and mirror symmetry about the vertical planes) that is essential for low-energy Dirac dispersion in the band structure.

Characterization of acoustic graphene

Similar to our earlier work, 32 we employ TMIM to study wave propagation on AIN membranes through the piezoelectric effect. As shown in Figure 1B, elastic waves at around 1 GHz are launched by the emitter IDT, which is tilted from the normal of the PnC by an angle α such that elastic waves inside the PnC can propagate in the horizontal direction. Details of the

Device Article



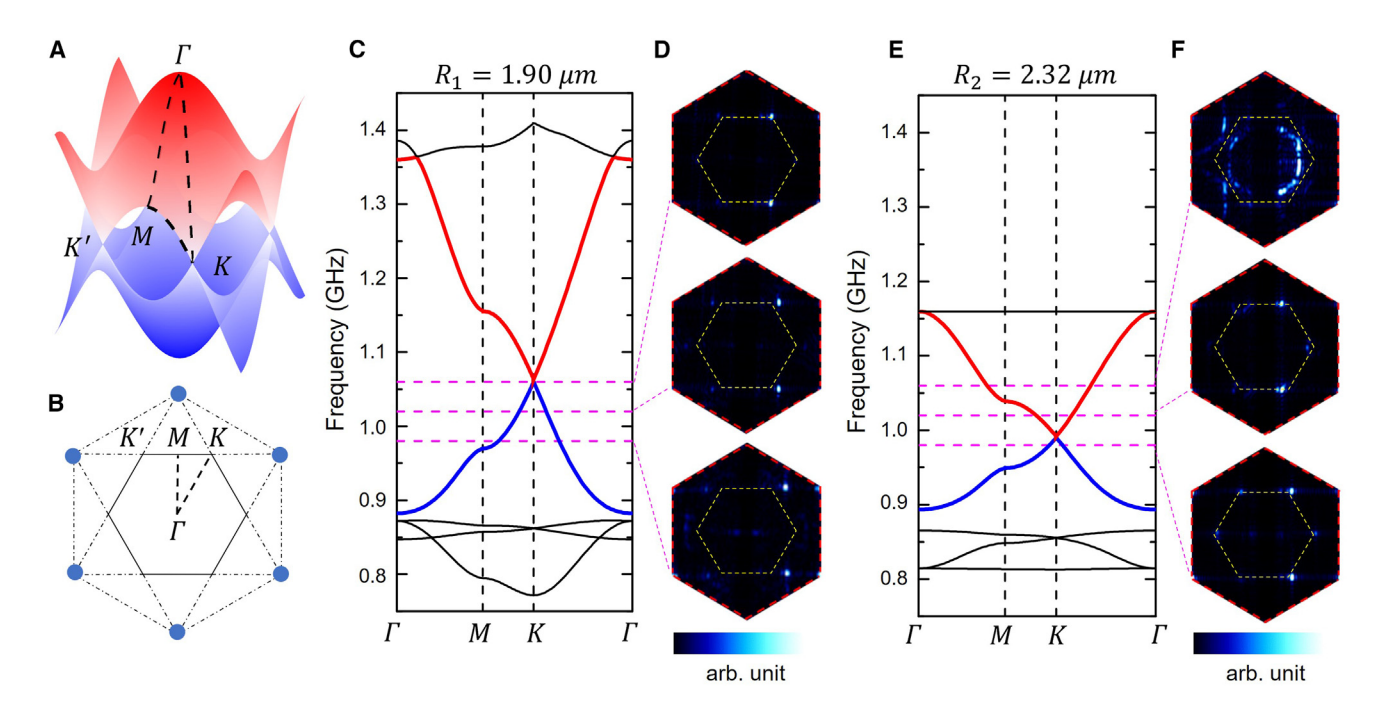


Figure 2. Simulated and measured phononic bands of two PnCs

- (A) Schematic 3D band structure of acoustic graphene.
- (B) Reciprocal-space map of the honeycomb lattice. The solid hexagon is the first Brillouin zone, with the high-symmetry points labeled in the map. The blue dots represent the reciprocal lattice sites.
- (C) Simulated band structure of sample #1 with R_1 = 1.90 μm .
- (D) k-space maps of sample #1 obtained by FFT of the TMIM data at 1.06, 1.02, and 0.98 GHz, as marked in (C). The first Brillouin zones are denoted by yellow dashed hexagons.

(E and F) Same as (C) and (D) for sample #2 with R_1 = 2.32 μ m.

momentum matching condition that determines the launching angle can be found in Note S2. The piezoelectric surface potential on AlN is detected by the cantilever probe, amplified by the TMIM electronics, and demodulated by an in-phase/quadrature (I/Q) mixer. 29,30 The technique detects the net effect of piezoelectric transduction from the vector (both out-of-plane and inplane) displacement fields to the GHz electrical potential on the sample surface. Signals at the radio-frequency (RF) and local-oscillator (LO) ports of the I/Q mixer can be expressed as $V_{\rm RF} \propto e^{i(\omega t - \vec{k} \cdot \vec{r})}$ and $V_{\rm LO} \propto e^{i\omega t}$, respectively, where ω is the angular frequency, and \vec{k} is the wave vector. The two output channels of the I/Q mixer are therefore $V_{\rm Ch1} \propto {\rm Re}(V_{\rm RF} V_{\rm LO}^*) = \cos(\vec{k} \cdot \vec{r})$ and $V_{\rm Ch2} \propto {\rm Im}(V_{\rm RF} V_{\rm LO}^*) = -\sin(\vec{k} \cdot \vec{r})$.

Figures 1C and 1D show the simultaneously taken atomic-force microscopy (AFM) and TMIM-Ch1 images, respectively (Note S3). It is clear that the TMIM is measuring the GHz potential rather than the surface topography. By combining the two TMIM output channels as $V_{\rm Ch1}+i*V_{\rm Ch2}$, we obtain phase-sensitive signals that are proportional to the displacement fields, from which the reciprocal-space (i.e., k-space) information can be extracted through fast-Fourier transformation (FFT). Such an approach will be exploited in our analysis below.

Figure 2A shows a schematic illustration of the 3D band structure in acoustic graphene, a prerequisite to emulate the Klein tunneling effect. In the following, we will follow the convention in

condensed matter physics to describe the phononic system. The unit cell (dashed rhombus in Figure 1A) of the honeycomb lattice consists of two sets of triangular sublattices, leading to the formation of linearly dispersed Dirac cones near the K and K'points of the Brillouin zone (Figure 2B, where the blue dots correspond to the reciprocal lattice sites). For single-layer graphene with sublattice pseudospin degree of freedom, the electron wavefunction at the barrier interface matches the corresponding hole wavefunction, which is known as the charge-conjugation symmetry. Fermions in single-layer graphene thus exhibit a chirality that resembles the half-integer spinor wavefunctions in quantum electrodynamics. Theoretical analysis 16,18 has shown that a massless Dirac electron normally incident on a translationally invariant potential cannot be backscattered. In other words, the electron velocity remains the same regardless of the presence of the barrier; i.e., it is conserved along the propagating direction. The two conditions^{16,18} for Klein tunneling are thus satisfied for single-layer graphene. Because of the analogy between electronic and phononic systems, Klein tunneling is expected for the acoustic graphene in our study.

The snowflake pattern offers multiple parameters for adjusting phononic bands, 31 such as the length R and width w of six arms and the lattice constant a_0 . We vary R to tune the position of the Dirac point, while keeping w=1 μm and $a_0=5.2$ μm unchanged in the design. Figure 2C shows the acoustic band structure of sample #1 with $R_1=1.90$ μm simulated by finite-element



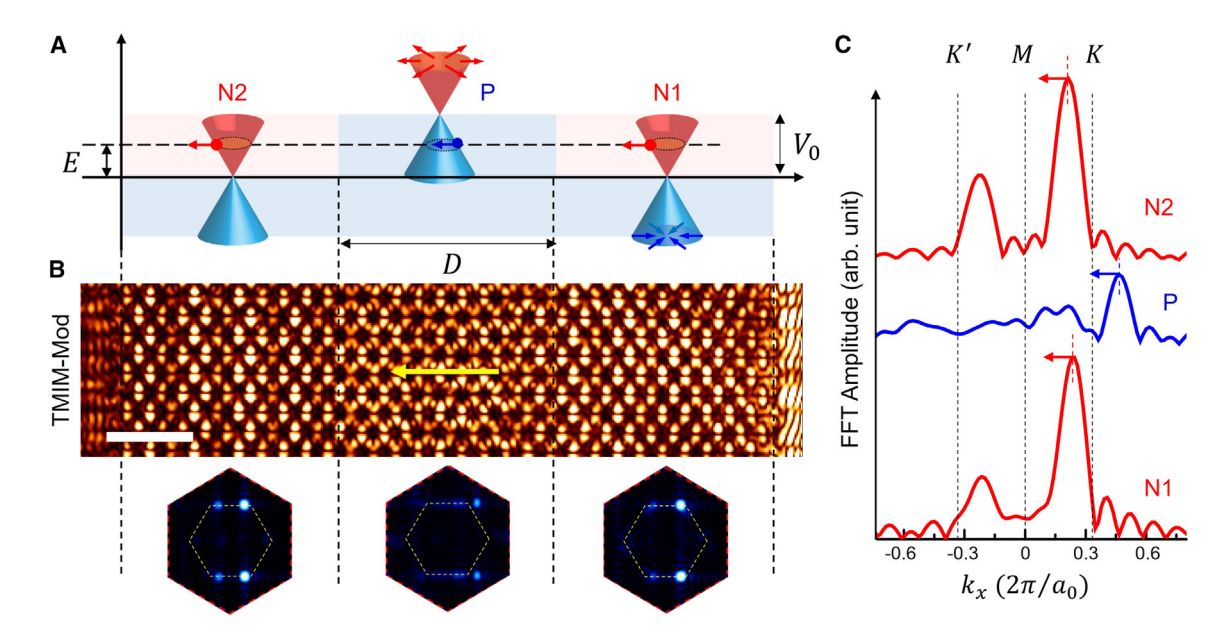


Figure 3. Acoustic Klein tunneling across the NPN sample

(A) Schematic of Klein tunneling of a Dirac quasiparticle with energy E across a potential barrier of width D and height V_0 . The three sections of the heterostructure are labeled by N1, P, and N2. Arrows represent the direction of pseudospin.

(B) TMIM modulus image and FFT maps in each section of sample #3 taken at f = 1.02 GHz. The scale bar represents 20 μ m.

(C) FFT line profiles along the K'-K direction in all three sections of the NPN sample. The peak in the P region corresponds to the propagating acoustic wave in the hole-like band. The peaks near the K' points are associated with waves reflected from the boundary of PnC.

modeling (see experimental procedures), where the K and lower M points are situated at 1.06 and 0.97 GHz, respectively. The full band structure of the phononic crystal starting from zero frequency, as well as the mode profiles in the vicinity of the Dirac cone, are shown in Note S4. Note that the Dirac-like linear dispersion no longer holds as the frequency approaches the M point. For comparison, we obtain the k-space maps by Fourier transformation of the TMIM data. For simplicity, we only present results near the 1st Brillouin zone and ignore FFT peaks in higherorder zones (Note S3). The FFT images in Figure 2D indicate that the Dirac point is indeed at 1.06 GHz, and the peaks move away from the K point at decreasing frequencies. Note that the sharp boundary of a rectangular real-space image will lead to the missing of information on the x axis and y axis of FFT data.³³ The third equivalent K point on the x axis is thus very weak due to such boundary effects. For sample #2 with R_2 = 2.32 μ m (Figure 2E), the calculated K and upper M points are at 1.00 and 1.04 GHz, respectively. The FFT images in Figure 2F confirm that f = 0.98 GHz is inside the valence band and 1.02 GHz inside the conduction band. At f = 1.06 GHz, the chemical potential is well above the M point. Correspondingly, the FFT image displays a semicircle within the 1st Brillouin zone, in good agreement with the simulated band structure. Complete FFT data for samples #1 and #2 can be found in Note S5.

Observation of acoustic Klein tunneling

With the successful tuning of Dirac frequencies in samples #1 and #2, we can now emulate the Klein tunneling effect in sample #3, which is formed by sandwiching a section of PnC with

 $R = R_1$ (Dirac point at 1.06 GHz) between two sections with $R = R_2$ (Dirac point at 1.00 GHz). For an excitation frequency between the two Dirac points, e.g., f = 1.02 GHz, the band alignment in Figure 3A resembles the negative-positive-negative (NPN) configuration in gated graphene devices. 19-22 Here, the electron-like quasiparticle with energy E = 20 MHz in the N-type region sees an effective potential barrier of $V_0 = 60$ MHz in the P-type region. Due to the one-to-one correspondence between velocity and sublattice pseudospin, formally known as momentum-pseudospin locking, Dirac quasiparticles cannot be backscattered to the other sublattice under normal incidence. 16,18 As a result, the expected transmission across the NPN heterojunction is unity even in the presence of a classically forbidden energy barrier. In our experiment, the TMIM modulus $(\sqrt{V_{\text{Ch1}}^2 + V_{\text{Ch2}}^2})$ image in Figure 3B indicates that the strength of the elastic wave is comparable on both sides of the potential barrier. For quantitative analysis, we perform FFT of the TMIM data in all three sections (Note S6) and plot the FFT line profiles along the K'-K direction in Figure 3C. Since we use the same tip and electronics to take the TMIM image and crop the same frame for Fourier transformation, the ratio of FFT peak heights between the two N-type sections provides a good measure of the transmission of acoustic wave, which is near unity from Figure 3C. Note that FFT peaks also appear near the K' valley, which are associated with the reflected wave due to impedance mismatch at the sharp interface between the PnC and unpatterned AIN membrane.

In theory, wave reflection at the PnC boundary can be suppressed using a tapered structure.³⁴ In reality, however,





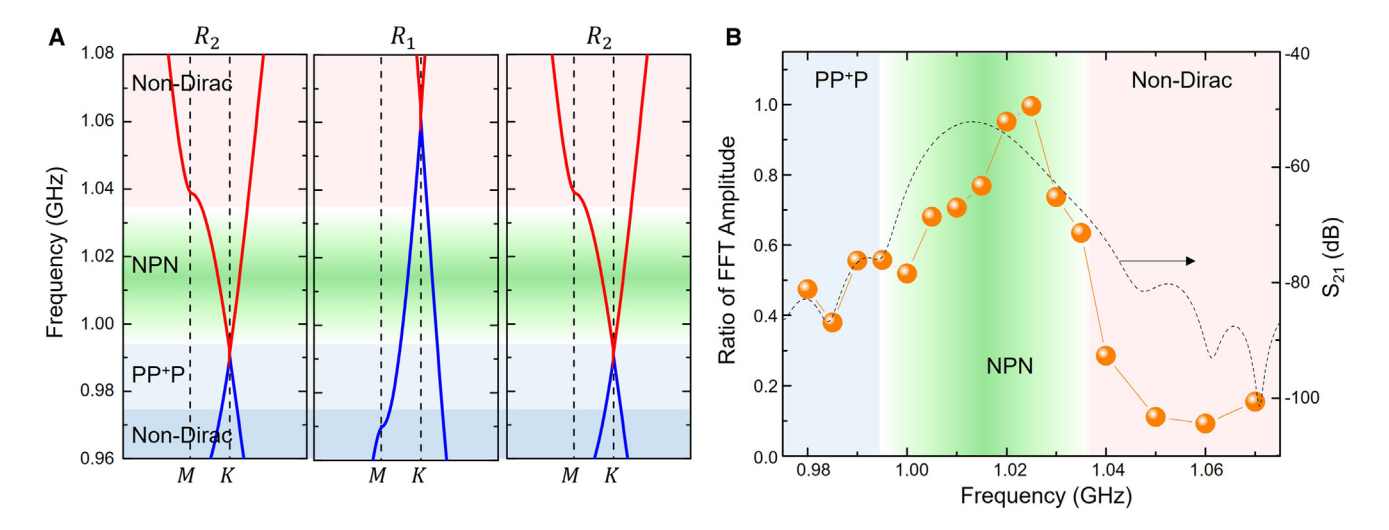


Figure 4. Frequency-dependent transmission under different band alignment conditions

(A) Close-up band alignment diagrams of sample #3 near the K points.

(B) Ratio of the FFT amplitude between the two $R = R_2$ sections, which is a measure of the transmission rate across the energy barrier. The transmission coefficient S_{21} measured by a network analyzer is also shown for comparison.

sufficient reduction of reflected waves requires a very long taper (Note S7), which is not practical in our current design. In addition, using network analysis of the transmission and reflection (Note S8), one can show that multiple reflections at the PnC boundary do not affect the measurement of transmission.³² The observation of unity transmission from N1 to N2 is also indicative of transparent hetero-interfaces without internal transmission and reflection (Note S8).

Figure 4A depicts the band alignment of sample #3 near the K points. Within our IDT passband of 0.98-1.07 GHz, there exist three regimes for the device. Below 1.00 GHz, all three sections of the sample are in the hole-like band, and the configuration is denoted as PP+P. In the frequency range between 1.00 and 1.03 GHz, the bands have NPN-like alignment, and Klein tunneling is expected to occur. For frequency above 1.035 GHz, the deviation from linear Dirac dispersion becomes significant in the $R = R_2$ section; i.e., the system becomes non-Dirac, and the conditions for Klein tunneling no longer exist. The TMIM data across the three regimes, as shown in Note S9, are consistent with this analysis. In particular, in the Klein tunneling regime, the wavefronts in all three sections are uniform and parallel to the propagation direction. In contrast, for both the PP+P and non-Dirac regimes, the wavefronts are distorted and less uniform across the sample.

For quantitative evaluation of the frequency-dependent wave transmission, we plot the ratio of FFT peak amplitudes between the two $R=R_2$ sections in Figure 4B. The ratio is around 0.5 in the PP+P configuration, approaches unity in the NPN regime, and drops sharply to below 0.2 for the non-Dirac dispersion. For comparison, we also show the timegated transmission coefficient S_{21} measured by a network analyzer between the two IDTs. Apart from the slight (\sim 5 MHz) difference between the frequency of S_{21} peak and that of maximum FFT ratio, which may be due to extrinsic effects in the RF circuit, the image analysis from TMIM data is in

good agreement with the terminal-to-terminal wave transmission. We note that near-unity transmission is only observed at the center of the NPN regime. In the snowflake design, the two sections with $R=R_1$ and $R=R_2$ exhibit very different bandwidths of the linear dispersion band, resulting in considerably different Fermi velocity that is proportional to the slope df/dk at the K point of the quasiparticle. While theoretically this does not change the unity transmission at normal incidence (see analysis below), it may, together with the multiple reflections at the PnC boundaries, affect the wave propagation close to the Dirac point. Further investigations are needed to understand the mechanism of reduction in wave transmission away from the center of the NPN regime.

Angular dependence of acoustic Klein tunneling

Finally, we investigate the angular dependence of Klein tunneling in our phononic devices. For quasiparticle tunneling through a rectangular energy barrier, the projection of its momentum parallel to the interface is conserved since translational invariance along this direction is not affected by the interface. 16,18 The consequence of this conservation law is that the transmission coefficient is strongly dependent on the incident angle ϕ . In other words, wave transmission is expected to be perfect only at $\phi = 0^{\circ}$ and to drop considerably as ϕ increases. To test this prediction, we constructed 6 devices with the same heterostructure as that in sample #3 but different launching angle α of the emitter IDT (Note \$10). The inset of Figure 5A shows the schematic of a particular device sample #4E with $\alpha = 19.5^{\circ}$. By analyzing the relevant wavevectors in Figure 5A, we can calculate the incident angle ϕ and refracted angle θ of group velocity on the N-type and P-type sides of the interface, respectively. Detailed k-space analysis of the wavevectors can be found in Note S10, where all angles are tabulated for clarity.

The TMIM-Ch1 image taken at f = 1.025 GHz and corresponding k-space maps of all three sections in sample #4E



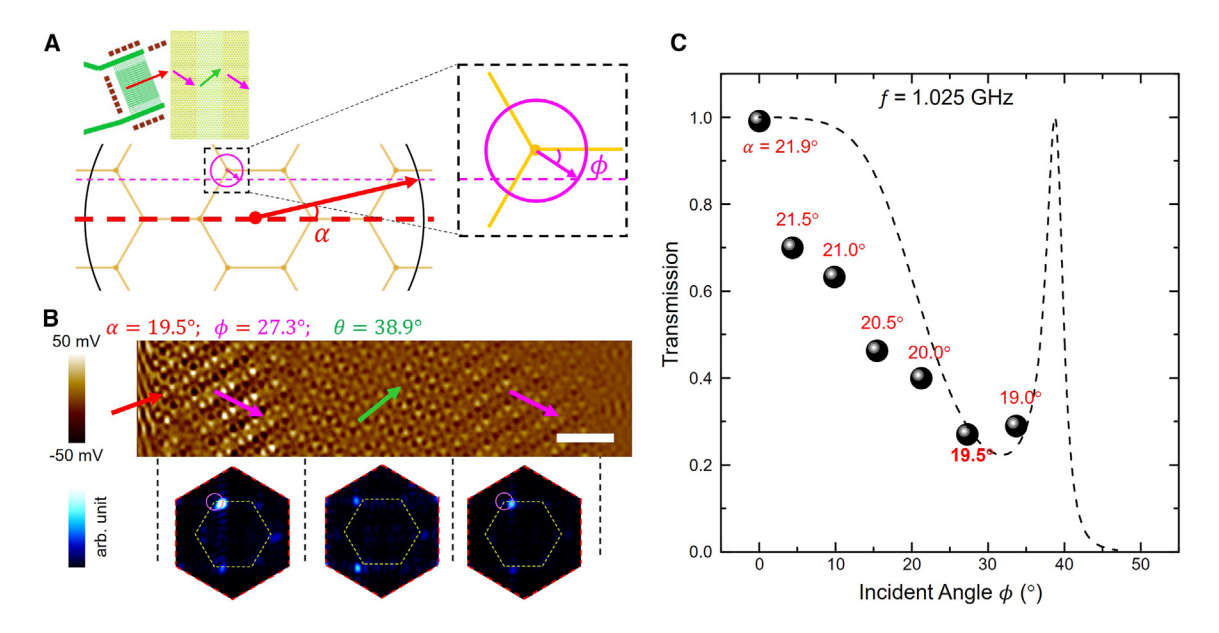


Figure 5. Angular dependence of acoustic Klein tunneling

(A) Reciprocal-space analysis of the incident angle ϕ . The hexagons denote the Brillouin zones. The magenta circle represents the isotropic dispersion near the Dirac point. The inset in the upper left shows the device configuration.

(B) TMIM-Ch1 image and FFT maps of all three sections of sample #4E taken at 1.025 GHz. Arrows indicate the direction of group velocity in each section. The scale bar represents 20 μm.

(C) Energy transmission rate as a function of the incident angle. The IDT angles are labeled next to the data points. The dashed line is the theoretical curve. The peak at $\phi = 38.8^{\circ}$ corresponds to the first-order resonant condition.

are displayed in Figure 5B. The theoretically calculated directions of group velocity in each section are marked in the image. A notable feature is that the refraction of Dirac quasiparticles across the heterojunction does not follow the conventional Snell's law. Instead, both the incident and refracted waves lie on the same side of the interface normal, which is the foundation of the Veselago focusing effect. 35,36 The complete set of TMIM data for all 6 devices is included in Note S11. Strikingly, a small change of the IDT launching angle from 21.9° to 19.5° leads to significant reduction in the wave transmission through the NPN heterostructure, as evident from the TMIM data. The positions and strengths of the FFT peaks also confirm the direction of wavevectors and the attenuation of transmitted waves. In Figure 5C, we plot the energy transmission rate (i.e., the square of the ratio between FFT amplitude of the peaks near K points in N2 and N1) as a function of the incident angle and compare the results with theoretical analysis (Note S12). The substantial drop of transmission under oblique incidence is clearly observed in our experiment, which can be utilized for angle-resolved filtering applications. It should be noted that ultra-fine control of the IDT angle well below 0.1° is needed to reach the first-order resonant condition with perfect transmission at the oblique incidence $\phi = 38.8^{\circ}$ (Note S12), which is very difficult for our current device design and fabrication.

Conclusions and outlook

We report the observation of Klein tunneling of GHz elastic waves in suspended piezoelectric membranes with graphene-

like phononic structures. The real-space profiles of the elastic waves are visualized by TMIM, from which the reciprocal-space information can be extracted by Fourier transformation and compared with simulated band structures. The near-unity transmission through an energy barrier under normal incidence is observed in the NPN-like heterostructure, whereas the transmitted wave is strongly attenuated outside this regime. By controlling the launching angle of elastic waves from the emitter IDT, we demonstrated the angular dependence of Klein tunneling in the same metamaterial design.

The realization of Klein tunneling in the GHz regime has profound implications for classical and quantum acoustic devices. For microwave signal processing, robust near-unity normal transmission is important for filtering applications. The strong angular dependence of the acoustic transmission demonstrated here will help suppress stray waves that unintentionally propagate on the device. As GHz phonons are widely utilized as information carriers in quantum computation systems, the capability of narrow-band filtering and angular waveguiding by Klein tunneling structures is desirable for the precise control of quantum transduction and information transportation. Finally, while the experimental demonstration is performed with a narrow filtering passband around 1 GHz in this work, the device fabrication and TMIM imaging can be easily extended to the 3-6 GHz regime^{37,38} for wireless telecommunication and quantum acoustic applications. In all, our work paves the way to exploit exotic high-energy-physics phenomena for classical waveguiding and integrated phononic circuit applications.

Please cite this article in press as: Lee et al., Klein tunneling of gigahertz elastic waves in nanoelectromechanical metamaterials, Device (2024), https://doi.org/10.1016/j.device.2024.100474





EXPERIMENTAL PROCEDURES

Resource availability

Lead contact

Further information and requests for resources and reagents should be directed to and will be fulfilled by the lead contact, Keji Lai (kejilai@physics.utexas.edu).

Material availability

This study did not generate new unique reagents.

Data and code availability

The datasets generated during the current study, and/or analyzed during the current study, are available from the corresponding author. This paper does not report the original code or a dataset generated by any code.

Device fabrication

The 800-nm-thick c-axis-oriented polycrystalline AlN films were provided by the Claire & John Bertucci Nanotechnology Laboratory at Carnegie Mellon University. The films were grown on 100-mm undoped <100> Si wafers with a nominal resistivity >20,000 Ω -cm. The wafers were loaded into a magnetron sputtering system with an S-gun arrangement, 39 which includes DC, AC, and RF components. The AC power is the primary power source. Before the AlN deposition, an argon sputter etch was performed for 180 s, which was designed to remove the native oxide on the Si wafer. The AlN deposition time was 549 s. The X-ray diffraction rocking curve of the thin films showed a full width at half maximum of 1.2°, indicative of a high degree of crystal orientation. 40 The phononic crystals consist of hexagonal arrays of etched six-armed snowflake patterns. The IDTs were formed by the deposition and overnight soak in Remover-1165 at room temperature to lift off the 45-nm Al films. The suspended AlN devices were released from silicon substrates with isotropic XeF2 etcher.

Numerical simulation

The numerical simulation is conducted by the commercial COMSOL Multiphysics software based on the finite-element method. The "Piezoelectric Effect Multiphysics" module is applied, which couples the "Solid Mechanics" module and "Electrostatics" module. The Bloch boundary conditions are imposed on the boundaries of unit cells in the simulation of band structures. The material properties used in the simulations are as follows: c11 = c22 = 375 GPa, c12 = 125 GPa, c13 = c23 = 120 GPa, c33 = 435 GPa, c44 = c55 = 118 GPa, c66 = (c11 - c12)/2 = 125 GPa, e31 = e32 = -0.58 C m^{-2}, e33 = 1.55 C m^{-2}, e15 = e24 = -0.48 C m^{-2}, and ρ = 3,100 kg m^{-3}.

Transmission-mode microwave impedance microscopy

The TMIM setup is implemented on an AFM platform (ParkAFM, XE-70). The shielded cantilever probe (Model 5-300N) is commercially available from PrimeNano. Details of the TMIM experiment can be found in Zheng et al.²⁹ All measurements are performed at room temperature.

SUPPLEMENTAL INFORMATION

Supplemental information can be found online at https://doi.org/10.1016/j.device.2024.100474.

ACKNOWLEDGMENTS

This work was primarily supported by the National Science Foundation Division of Engineering Awards ECCS-2221822 and ECCS-2221326 and partially by the Gordon and Betty Moore Foundation, grant https://doi.org/10.37807/gbmf12238, and the Welch Foundation grant F-1814. The device fabrication work was carried out in part at the Singh Center for Nanotechnology, part of the National Nanotechnology Coordinated Infrastructure Program, which is supported by the National Science Foundation grant NNCI-1542153.

AUTHOR CONTRIBUTIONS

Q.Z., A.T.C.J., and K.L. conceived the project. Q.Z. and Y.J. fabricated the phononic devices and performed band structure simulations. D.L. performed

the TMIM imaging and data analysis. X.Z. and S.J. contributed to the TMIM data analysis. C.W. contributed to the phononic crystal design. D.L. and K.L. drafted the manuscript with contributions from all authors. All authors have given approval to the final version of the manuscript.

DECLARATION OF INTERESTS

The authors declare no competing interests.

Received: May 28, 2024 Revised: June 18, 2024 Accepted: July 8, 2024 Published: August 7, 2024

REFERENCES

- Soukoulis, C.M., and Wegener, M. (2011). Past achievements and future challenges in the development of three-dimensional photonic metamaterials. Nat. Photonics 5, 523–530. https://doi.org/10.1038/nphoton. 2011.154.
- Cummer, S.A., Christensen, J., and Alù, A. (2016). Controlling sound with acoustic metamaterials. Nat. Rev. Mater. 1, 1–13. https://doi.org/10.1038/ natreymats.2016.1.
- Gao, P., Torrent, D., Cervera, F., San-Jose, P., Sánchez-Dehesa, J., and Christensen, J. (2019). Majorana-like zero modes in Kekulé distorted sonic lattices. Phys. Rev. Lett. 123, 196601. https://doi.org/10.1103/PhysRev-Lett.123.196601.
- Xu, J.S., Sun, K., Han, Y.J., Li, C.F., Pachos, J.K., and Guo, G.C. (2016). Simulating the exchange of Majorana zero modes with a photonic system. Nat. Commun. 7, 13194. https://doi.org/10.1038/ncomms13194.
- Wang, K., Dutt, A., Wojcik, C.C., and Fan, S. (2021). Topological complexenergy braiding of non-Hermitian bands. Nature 598, 59–64. https://doi. org/10.1038/s41586-021-03848-x.
- Zhang, X., Zangeneh-Nejad, F., Chen, Z.G., Lu, M.H., and Christensen, J. (2023). A second wave of topological phenomena in photonics and acoustics. Nature 618, 687–697. https://doi.org/10.1038/s41586-023-06163-9.
- Lu, L., Joannopoulos, J.D., and Soljačić, M. (2014). Topological photonics. Nat. Photonics 8, 821–829. https://doi.org/10.1038/nphoton.2014.248.
- Ozawa, T., Price, H.M., Amo, A., Goldman, N., Hafezi, M., Lu, L., Rechtsman, M.C., Schuster, D., Simon, J., Zilberberg, O., and Carusotto, I. (2019). Topological photonics. Rev. Mod. Phys. 91, 015006. https://doi.org/10.1103/RevModPhys.91.015006.
- Ma, G., Xiao, M., and Chan, C.T. (2019). Topological phases in acoustic and mechanical systems. Nat. Rev. Phys. 1, 281–294. https://doi.org/10. 1038/s42254-019-0030-x.
- Liu, Y., Chen, X., and Xu, Y. (2020). Topological phononics: from fundamental models to real materials. Adv. Funct. Mater. 30, 1904784. https://doi.org/10.1002/adfm.201904784.
- Klein, O. (1929). Die reflexion von elektronen an einem potentialsprung nach der relativistischen dynamik von Dirac. Z. Phys. 53, 157–165. https://doi.org/10.1007/BF01339716.
- Calogeracos, A., and Dombey, N. (1999). History and physics of the Klein paradox. Contemp. Phys. 40, 313–321. https://doi.org/10.1080/00107 5199181387.
- Dombey, N., and Calogeracos, A. (1999). Seventy years of the Klein paradox. Phys. Rep. 315, 41–58. https://doi.org/10.1016/S0370-1573(99)00023-X.
- Griffiths, D.J., and Schroeter, D.F. (2018). Introduction to Quantum Mechanics (Cambridge university press).
- Beenakker, C.W.J. (2008). Colloquium: Andreev reflection and Klein tunneling in graphene. Rev. Mod. Phys. 80, 1337–1354. https://doi.org/ 10.1103/RevModPhys.80.1337.

Please cite this article in press as: Lee et al., Klein tunneling of gigahertz elastic waves in nanoelectromechanical metamaterials, Device (2024), https://doi.org/10.1016/j.device.2024.100474





- Allain, P.E., and Fuchs, J.N. (2011). Klein tunneling in graphene: optics with massless electrons. Eur. Phys. J. B 83, 301–317. https://doi.org/10.1140/ epjb/e2011-20351-3.
- Novoselov, K.S., Geim, A.K., Morozov, S.V., Jiang, D., Katsnelson, M.I., Grigorieva, I.V., Dubonos, S., and Firsov, A.A. (2005). Two-dimensional gas of massless Dirac fermions in graphene. Nature 438, 197–200. https://doi.org/10.1038/nature04233.
- Katsnelson, M.I., Novoselov, K.S., and Geim, A.K. (2006). Chiral tunnelling and the Klein paradox in graphene. Nat. Phys. 2, 620–625. https://doi.org/ 10.1038/nphys384.
- Huard, B., Sulpizio, J.A., Stander, N., Todd, K., Yang, B., and Goldhaber-Gordon, D. (2007). Transport measurements across a tunable potential barrier in graphene. Phys. Rev. Lett. 98, 236803. https://doi.org/10.1103/PhysRevLett.98.236803.
- Gorbachev, R.V., Mayorov, A.S., Savchenko, A.K., Horsell, D.W., and Guinea, F. (2008). Conductance of pnp graphene structures with "airbridge" top gates. Nano Lett. 8, 1995–1999. https://doi.org/10.1021/ nl801059v.
- Stander, N., Huard, B., and Goldhaber-Gordon, D. (2009). Evidence for Klein tunneling in graphene p— n junctions. Phys. Rev. Lett. 102, 026807. https://doi.org/10.1103/PhysRevLett.102.026807.
- Young, A.F., and Kim, P. (2009). Quantum interference and Klein tunnelling in graphene heterojunctions. Nat. Phys. 5, 222–226. https://doi.org/10. 1038/nphys1198.
- Dreisow, F., Keil, R., Tünnermann, A., Nolte, S., Longhi, S., and Szameit, A. (2012). Klein tunneling of light in waveguide superlattices. Europhys. Lett. 97, 10008. https://doi.org/10.1209/0295-5075/97/10008.
- Zhang, Z., Feng, Y., Li, F., Koniakhin, S., Li, C., Liu, F., Zhang, Y., Xiao, M., Malpuech, G., and Solnyshkov, D. (2022). Angular-dependent Klein tunneling in photonic graphene. Phys. Rev. Lett. 129, 233901. https:// doi.org/10.1103/PhysRevLett.129.233901.
- Jiang, X., Shi, C., Li, Z., Wang, S., Wang, Y., Yang, S., Louie, S.G., and Zhang, X. (2020). Direct observation of Klein tunneling in phononic crystals. Science 370, 1447–1450. https://doi.org/10.1126/science.abe2011.
- Gao, N., Wang, J., and Chen, W. (2022). Klein tunneling for Lamb waves in elastic phononic crystal plates. Appl. Phys. Lett. 121, 102201. https://doi. org/10.1063/5.0105897.
- Zhu, Y., Merkel, A., Cao, L., Zeng, Y., Wan, S., Guo, T., Su, Z., Gao, S., Zeng, H., Zhang, H., and Assouar, B. (2023). Experimental observation of super-Klein tunneling in phononic crystals. Appl. Phys. Lett. 122, 211701. https://doi.org/10.1063/5.0151336.
- Zhang, X., and Liu, Z. (2008). Extremal Transmission and Beating Effect of Acoustic Waves in Two-Dimensional Sonic Crystals. Phys. Rev. Lett. 101, 264303. https://doi.org/10.1103/PhysRevLett.101.264303.

- Zheng, L., Wu, D., Wu, X., and Lai, K. (2018). Visualization of surfaceacoustic-wave potential by transmission-mode microwave impedance microscopy. Phys. Rev. Appl. 9, 061002. https://doi.org/10.1103/PhysRevApplied.9.061002.
- Zheng, L., Shao, L., Loncar, M., and Lai, K. (2020). Imaging acoustic waves by microwave microscopy: Microwave impedance microscopy for visualizing gigahertz acoustic waves. IEEE Microw. Mag. 21, 60–71. https://doi. org/10.1109/MMM.2020.3008240.
- Zhang, Z., Tian, Y., Christensen, J., Cheng, Liu, X., and Christensen, J. (2017). Experimental verification of acoustic pseudospin multipoles in a symmetry-broken snowflake-like topological insulator. Phys. Rev. B 96, 241306, (R). https://doi.org/10.1103/PhysRevB.96.241306.
- Zhang, Q., Lee, D., Zheng, L., Ma, X., Meyer, S.I., He, L., Ye, H., Gong, Z., Zhen, B., Lai, K., and Johnson, A.C. (2022). Gigahertz topological valley Hall effect in nanoelectromechanical phononic crystals. Nat. Electron. 5, 157–163. https://doi.org/10.1038/s41928-022-00732-y.
- Dong, Y., Jiao, W., Long, T., Liu, L., and He, G. (2019). Eliminating the effect of image border with image periodic decomposition for phase correlation based remote sensing image registration. Sensors 19, 2329. https://doi.org/10.1109/IGARSS.2018.8517570.
- Zheng, M., Park, C.I., Liu, X., Zhu, R., Hu, G., and Kim, Y.Y. (2020). Nonresonant metasurface for broadband elastic wave mode splitting. Appl. Phys. Lett. 116, 171903. https://doi.org/10.1063/5.0005408.
- Cheianov, V.V., Falko, V., and Altshuler, B.L. (2007). The focusing of electron flow and a Veselago lens in graphene pn junctions. Science 315, 1252–1255. https://doi.org/10.1126/science.1138020.
- Lee, G.H., Park, G.H., and Lee, H.J. (2015). Observation of negative refraction of Dirac fermions in graphene. Nat. Phys. 11, 925–929. https://doi.org/10.1038/nphys3460.
- Lee, D., Liu, Q., Zheng, L., Ma, X., Li, H., Li, M., and Lai, K. (2021). Direct visualization of gigahertz acoustic wave propagation in suspended phononic circuits. Phys. Rev. Appl. 16, 034047. https://doi.org/10.1103/Phys-RevApplied.16.034047.
- Lee, D., Jahanbani, S., Kramer, J., Lu, R., and Lai, K. (2023). Nanoscale Imaging of super-high-frequency microelectromechanical resonators with femtometer sensitivity. Nat. Commun. 14, 1188. https://doi.org/10.1038/s41467-023-36936-9.
- Felmetsger, V.V., Laptev, P.N., and Tanner, S.M. (2009). Design, operation mode, and stress control capability of S-Gun magnetron for ac reactive sputtering. Surf. Coating. Technol. 204, 840–844. https://doi.org/10. 1016/j.surfcoat.2009.08.007.
- Zaghloul, U., and Piazza, G. (2014). Synthesis and characterization of 10 nm thick piezoelectric AIN films with high c-axis orientation for miniaturized nanoelectromechanical devices. Appl. Phys. Lett. 104, 253101. https://doi.org/10.1063/1.4882240.